Available online at www.sciencedirect.com
ScienceDirect
Applied Catalysis B: Environmental 83 (2008) 85–95
APPLIED CATALYSIS B: ENVIRONMENTAL
www.elsevier.com/locate/apcatb

Lanthanum cobaltite catalysts for diesel soot combustion

Nunzio Russo, Stefania Furfori, Debora Fino *, Guido Saracco, Vito Specchia

Department of Materials Science and Chemical Engineering Politecnico di Torino, Corso Duca degli Abruzzi 24, 10129 Torino, Italy

Received 16 November 2007; received in revised form 7 February 2008; accepted 9 February 2008
Available online 15 February 2008

Abstract

This paper deals with the preparation (by solution combustion synthesis), the characterization (by XRD, AAS, BET, FESEM, XPS and TPD/R analyses), the catalytic activity evaluation (in a temperature-programmed combustion microreactor), and the conception of a possible reaction mechanism of a series of nano-structured soot combustion catalysts based on La–Co substoichiometric or alkali metal-substituted perovskites ($La_{0.9}CoO_3$, $La_{0.9}Na_{0.1}CoO_3$, $La_{0.9}K_{0.1}CoO_3$, $La_{0.9}Rb_{0.1}CoO_3$), whose performance has been compared with that of the standard $LaCoO_3$. Significant catalytic activities have been measured in the 350–450 °C range, even after a specific thermal ageing protocol (at 850 °C for 16 h in the presence of water) or repeated combustion cycles (up to 9). The $La_{0.9}Rb_{0.1}CoO_3$ catalyst has been found to allow the best compromise between satisfactory catalytic activity and stability. This catalyst has been then deposited on an SiC wall-flow trap, submitted to the same ageing treatment and then tested on a diesel engine bench (trap loading and regeneration inducing a temperature increase due to the catalytic combustion of the on purpose post-injected fuel). The presence of the catalyst in the wall-flow trap has enabled both a more complete regeneration and a significant reduction of the regeneration time compared to that of a non-catalytic trap, even after ageing, with a consequent potential saving of post-injected fuel.

Keywords: Alkali-substituted lanthanum cobaltites; Perovskite; Catalytic combustion; Diesel particulate; Soot

1. Introduction

Road transport is a major contributor to the emissions of various greenhouse gases and has a significant share in the emission of harmful hydrocarbons (HC), nitrogen oxides (NOx) and particulate matter (PM). PM, in particular, is responsible for a number of respiratory diseases [1]. The market share of diesel passenger cars currently exceeds 40% of new vehicle registrations and will most likely reach 50% of the market in Europe in the near future [2]. In comparison to gasoline vehicles, the control of exhaust emissions from diesel engines is at a relatively early stage of development. A combination of engine modifications and after-treatment technologies is suggested to achieve compliance with future very severe legislative limits [3]. Clean emissions have to be achieved without significantly affecting the high thermal efficiency that is a distinctive feature of diesel engines.

The key methods for exhaust emission control lie in a combination of exhaust gas recirculation (EGR), high-pressure fuel injection (common-rail systems), diesel particulate filters (DPF) and catalyst technologies (combustion of CO, HC and soot, selective reduction of nitrogen, etc.) [4].

The prevalent technology available to control diesel particulate emissions is in put the use of filters to capture soot particles from the exhaust stream. The filters must be regenerated periodically, or continuously, by trapped soot combustion in order to prevent unacceptable back-pressure increases [5,6]. During most diesel engine operations, the exhaust gas temperatures remain rather too low (about 250 °C) to promote continuous un-catalysed particulate matter (PM) oxidation [7]. Therefore, auxiliary systems, such as an electrical heater or a fuel burner, must be installed to ignite trapped diesel soot. These auxiliary systems are designed to heat the exhaust gases to the regeneration temperature (>600 °C), and consequently, this operation is exposed to a certain risk, because of the rather high temperatures that have to be handled, and is characterized by an associated energy consumption. Conversely, the combustion temperature of diesel particulate matter can be lowered using a specific oxidation

* Corresponding author. Tel.: +39 011 090 4710; fax: +39 011 090 4699.
E-mail address: debora.fino@polito.it (D. Fino).

0926-3373/$ – see front matter © 2008 Elsevier B.V. All rights reserved.
doi:10.1016/j.apcatb.2008.02.006

catalyst. Catalytic filter regeneration reduces the operational risk and the energy consumption to such a level that regeneration without employing auxiliary systems could even be attempted, even though the huge amount of research carried out so far has not brought about this quite amenable result. The catalyst can be lined over the filter walls. The performance of the derived catalytic traps is affected by the intrinsic catalytic activity and the soot–catalyst contact effectiveness, which in turn is influenced by the relative concentration of the solids and the catalyst morphology.

Several authors have carried out studies on the reduction of diesel particulate emissions using catalysts for the combustion of trapped soot [8–10]. It has been shown that the adoption of a catalyst can lead to a more complete regeneration of the trap and to lower energy consumption (e.g. fuel penalties) during the regeneration process. Several kinds of catalysts have been tested: perovskite type oxides [11–14], spinel type oxides [15,16], alkaline or heavy metal oxides [17–21], mixtures of halides with vanadates or molibdates [22–24], precious metals [25,26]. A comparison of the performances of the different catalysts proposed to date should be made bearing in mind that not only the catalytic activity, but also several other characteristics, should be taken into account: thermal stability, chemical reactivity towards both the ceramic supports and the chemical species contained in the emissions, costs, etc.

The direct catalytic combustion of diesel particulate is a process that is based on a heterogeneous reaction involving solid particles of soot, gaseous oxygen and, of course, the solid catalyst. In order to promote this combustion, the catalyst must be in contact with soot particles. This may actually be favoured by the synthesis of foamy microstructures of nano-sized catalyst crystals, such as those usually obtained from solution combustion synthesis (SCS) methods [27–29]. Furthermore, the interaction between the catalyst and the oxygen contained in diesel exhausts is believed to play an important role on the combustion of soot, in particular when the catalyst acts as an oxygen pump and it even promotes oxygen spill-over [23].

Generally speaking, combustion synthesis can be considered as a cheap, energy saving and fast route to obtain foamy nano-structured powders of oxides; for these reasons, this technique has been widely applied to the preparation of a large number of different compounds [31].

In the present paper, the activity of promising SCS-synthesized perovskite catalysts belonging to the lanthanum cobaltite family, has been investigated to complement some earlier studies by the authors on other mixed oxides catalysts [9,12–14,16,23]. A tentative reaction mechanism has been proposed. On the basis of the obtained results, the suitability of the mentioned catalysts for application in the treatment of actual diesel exhausts has also been discussed.

2. Experimental

2.1. Catalyst preparation

A series of perovskite catalysts ($LaCoO_3$, $La_{0.9}CoO_3$, $La_{0.9}Na_{0.1}CoO_3$, $La_{0.9}K_{0.1}CoO_3$, $La_{0.9}Rb_{0.1}CoO_3$) were prepared by SCS from an aqueous solution of nitrates (acting as oxidizers) and urea (acting as a sacrificial fuel). According to this method, the reagents (Fluka extra pure grade) are first dissolved in distilled water in stoichiometric amounts. The obtained solution is then placed into an oven kept at a constant temperature (600 °C) in air. The solution is quickly brought to the boil; it then froths and swells until the chemical reaction starts. Combustion is over in a few seconds, resulting in easily crumbling foam of nano-sized particles with a large specific volume and surface area [27].

Taking the $LaCoO_3$ synthesis as an indication, the combustion synthesis involving lanthanum nitrate, cobalt nitrate and urea occurs according to the following overall reaction which gives rise to a perovskite powder and gaseous species:

$$2La(NO_3)_3 + 2Co(NO_3)_2 + 8CO(NH_2)_2 \rightarrow 2LaCoO_3 + 8CO_2 + 13N_2 + 16H_2O \quad (1)$$

The whole reaction can be formally regarded as the combination of two different contributions:

$$2La(NO_3)_3 + 2Co(NO_3)_2 \rightarrow 2LaCoO_3 + 12O_2 + 5N_2 \quad (2)$$

$$8CO(NH_2)_2 + 12O_2 \rightarrow 8CO_2 + 16H_2O + 8N_2 \quad (3)$$

The exothermic reaction (3), namely urea combustion, provides the heat that is necessary for the completion of the decomposition reaction (2), i.e. the endothermic transformation of nitrate into the desired oxide.

This method, suitably adapted according to an *in situ* version, has also been demonstrated to be amenable for the deposition of mixed catalyst oxides in wall-flow diesel particulate traps based on SiC or cordierite [30].

2.2. Catalyst characterization

A compositional analysis (dissolution in HNO_3/HCl followed by atomic absorption analysis with a PerkinElmer 1100B spectrometer) was performed on all the prepared samples to check their elemental composition.

The catalysts were then analyzed by X-ray diffraction (PW1710 Philips diffractometer equipped with a monochromator, Cu Kα radiation) in order to assess their purity, crystalline structure and approximate crystal grain size. The same instrument, equipped with a specific hot chamber, was used to show the occurrence of phase transformations at temperatures ranging from 25 to 900 °C under a reducing mixture flow of 5% H_2 in Ar.

A field emission scanning electron microscope (FESEM-Leo 50/50 VP with a GEMINI column) was employed to analyze the microstructure of the crystal catalyst aggregates of the catalysts as well as the shape and size of the single perovskite crystals.

The BET-specific surface area of the catalysts has evaluated from the linear parts of the BET plot of the N_2 isotherms via a Micromeritics ASAP 2010 analyzer.

Finally, X-ray photoelectron spectroscopy was used to characterize the surface composition of the most active catalysts.

The XPS analyses were carried out with a VG Escalab 200-C X-ray photoelectron spectrometer employing a non-monochromatic Mg Kα source. A pass energy of 20 eV, a resolution of 1.1 eV, and a step of 0.2 eV were used to obtain high-resolution XPS spectra. The effects of sample charging were eliminated by referring the spectral line shift to the C 1s binding energy value of 284.6 eV. The XPS measurements were performed on the catalysts after two different thermal treatments: 60 min at 600 °C in pure oxygen with a pressure value of 1.1 bar (oxidizing condition) and 2 h at 400 °C in an ultra-high vacuum ($<2 \times 10^{-9}$ mbar; reducing condition) [12].

2.3. Carbonaceous materials

Various properties of carbon blacks, such as particle size and graphitic structure have been reported to be very similar to those of diesel soot, due to their similar formation mechanism, based on the combustion of carbonaceous fuels under substoichiometric conditions. As a result, commercially available carbon blacks have traditionally been used as diesel soot surrogates in order to study soot behaviour at a laboratory scale [31–33].

The catalytic activity of the catalysts towards carbon black combustion was investigated. A commercial carbon (Printex U by Degussa, a carbonaceous material which, contrary to soot, contains much less adsorbed hydrocarbons: 5 wt% [34]) was used. This type of carbon was selected because of its rather standard composition and because it burns at temperatures rather close to, but generally higher than those that are characteristic of diesel particulate combustion. These features make the achieved results, on the one hand, reproducible and on the other conservative with respect to a potential practical application.

2.4. Catalytic activity tests

The catalytic activity of the catalysts was tested in a temperature-programmed combustion (TPC) apparatus. This equipment consists of a fixed bed inserted into a quartz microreactor (i.d.: 4 mm). The fixed bed was prepared by mixing 50 mg of a 1:9 by weight mixture of Printex U and a powdered catalyst treated in a colloidal mill for 15 min, with 150 mg of silica pellets (0.3–0.7 mm in size); these inert pellets were added in order to reduce the specific pressure drop across the reactor and to prevent thermal runaways. The close (tight) contact conditions between the catalyst and the carbon obtained in the ball mill allow good reproducibility which is a *conditio sine qua non* to draw reliable comparisons between the intrinsic activity of different catalysts. However, these contact conditions are not representative of the real catalyst–soot contact conditions in the catalytic wall-flow application here pursued. Loose contact conditions, obtained by gently shaking the soot and catalyst powders in a vessel, provided a better approximation of the contact conditions of the soot accumulated in a catalyst-lined trap [30]. For this reason, a TPC run was also performed with a loose contact mixture of soot and the various catalysts that had been prepared.

The TPC reactor temperature was controlled through a PID-regulated oven and it was increased during a TPO run from 200 to 700 °C at a 5 °C/min rate, under an airflow of 100 N ml/min. The analysis of the reactor outlet gas was performed by means of a CO_2/CO NDIR analyzer (ABB). A computer was used to record both the fixed-bed temperature (measured by a thermocouple placed close to the sample) and the concentration of CO_2 in the outlet gas as a function of time (i.e. vs. the programmed temperature). The temperature corresponding to the CO_2 concentration peak (T_p) was taken as an index of the catalytic activity of each tested catalyst: the lower the T_p value, the higher the catalytic activity.

A TPC run was also performed in the absence of the catalyst in order to set a reference for comparison purposes. On the grounds of the area of the TPC plots, estimates of the overall CO_2 amount produced per run were calculated and the selectivity of carbon combustion towards CO_2 was also estimated.

2.5. Catalyst ageing procedure

In line with earlier investigations on other soot-combustion catalysts [35], a thermal ageing treatment was performed at 850 °C for 16 h under wet air, containing 30 vol% of moisture obtained by humidification in a thermostasized bubble column on the best catalyst selected, that is, $La_{0.9}Rb_{0.1}CoO_3$.

Further runs were then performed in order to check whether the catalyst remains stable after repeated carbon combustion cycles. In these runs, the catalyst was mixed, by gentle shaking in a vessel, with carbon (catalyst/carbon weight ratio = 9:1, loose and tight contact conditions) and kept at 500 °C under calm air for 2 h (a time sufficient to completely burn out the entire carbon amount). This treatment was repeated for nine combustion cycles. After each combustion cycle, a portion of the catalyst was used to perform a standard TPC run in order to detect any possible variation of the catalytic activity.

Most of the previously described physical and chemical characterization analyses described above were replicated on the aged samples.

2.6. Activation energy assessment by the Starink method

The activation energy of soot combustion over the prepared catalysts was measured according the Starink method [36], using differential scanning calorimetry (DSC) runs carried out in PerkinElmer DSC-Pyris equipment. Ten milligrams of a 2/1 by weight catalyst/carbon mixture were analyzed in the temperature range of 50–720 °C, scanned at different heating rates (1, 2, 4, and 8 °C/min). An airflow (100 ml/min) provided the oxygen required for carbon combustion. The DSC patterns were processed, thus obtaining the onset and the maximum temperatures of the exothermic combustion peak. The temperatures corresponding to the cumulative combustion of progressive soot amounts of 5–95 wt% (scanning step: 5 wt%) of the total carbon amount put in the sample holder were also determined through simple calculations. DSC scans were also performed (according to the experimental conditions reported above) on an alumina/carbon mixture, so as to estimate the activation energy of the non-catalysed combustion of carbon.

The so-called Starink procedure can be used to estimate activation energy estimation through a proper interpretation of the thermal analysis data. According to this method, the following relationship links the values of the heating rate (β) to the corresponding temperature values (T_α) at which a fixed fraction α of carbon is burned during each run:

$$\ln\left(\frac{\beta}{T_\alpha^{1.92}}\right) = -1.0008\frac{E_\alpha}{RT_\alpha} + \cos t$$

If the heat released by the combustion is assumed to be proportional to the fraction α of the converted carbon, the T_α value corresponding to such a value can easily be derived from the DSC curves by evaluating, via a simple integration, the amount of heat released by combustion. Estimates of the activation energy can be obtained from the slope of the best-fitting line [36], using a least-square fitting of the ln β-vs.-1/T_α data series.

2.7. Temperature-programmed desorption/reduction analyses

Some temperature-programmed analyses were performed in a Thermoquest TPD/R/O 1100 analyzer, equipped with a thermal conductibility detector (TCD).

A fixed catalyst bed was enclosed in a quartz tube and sandwiched between two quartz wool layers; prior to each temperature-programmed oxygen desorption (TPD) run, the catalyst was heated under an O_2 flow (40 N ml/min) to up to 750 °C. After 30 min at this temperature, which is a common pre-treatment, the temperature was lowered to 25 °C under the same oxygen flow rate, thereby achieving complete saturation. Afterwards, He was fed to the reactor at a 10 ml/min flow rate and kept for 1 h at room temperature in order to purge any excess oxygen. The catalyst was then heated to 950 °C at a constant heating rate of 10 °C/min under the same helium flow. The total amount of O_2 desorbed during the heating protocol was detected by the TCD detector after proper calibration.

Temperature-programmed reduction (TPR) experiments were also carried out in the same apparatus. After the same oxidation pre-treatment adopted for the TPD runs, the sample was reduced with a 4.95% H_2/Ar mixture (10 N ml/min), and meanwhile heated at a 10 °C/min rate up to 950 °C. Some runs were performed with different heating rates (1, 5 and 10 °C/min). Once again, the amount of converted H_2 was monitored via the TCD detector. A specific cold trap was placed before the TCD detector in order to prevent water from interfering. X-ray diffraction was carried out on the catalysts which underwent each TPD or TPR analysis to check whether the perovskite structure had been retained or not, and to detect the possible appearance of new phases.

2.8. Catalytic filter preparation and diesel engine bench tests

The best selected catalyst ($La_{0.9}Rb_{0.1}CoO_3$) was directly deposited by *in situ* SCS over the wall-flow filters. The ceramic support was dipped in the aqueous solution of its precursors and then placed into an oven heated to 600 °C. The aqueous phase was rapidly brought to boil, the water evaporated, the precursor mixture ignited and the synthesis reaction induced *in situ*. The selected support was a silicon carbide (SiC) filter produced by NGK (cell structure = 17/200; diameter 35 mm; length = 10 in.; pore diameter of the channel walls = 23 μm; porosity of the channel walls = 52%) which was found to be chemically compatible with the selected catalyst. The load of the deposited catalyst was assessed through gravimetric analysis and resulted equal to about 5 wt%.

The developed filter was tested on real diesel exhaust gases on an engine bench (Iveco F1C Unijet four cylinders, 3000 cm^3, 122 kW at 3500 rpm, maximum torque 380 Nm), where the temperature and gas composition upstream and downstream from the trap can be controlled and monitored, as well as the evolution of the pressure drop through the trap (a sign of soot accumulation). The gas hourly space velocity (GHSV) along the trap was 65,000 h^{-1}.

In line with the pending "EURO 5" regulations, all the tests were carried out using a low-sulphur (<50 ppmw) diesel fuel produced by Agip Petroli.

The following standard bench test procedure was adopted. The filter was loaded by letting comparatively cold exhaust gases flow through it until a 170 mbar pressure drop was reached. Then, regeneration was induced by post-injecting some fuel (0.025 kg fuel/kg of exhaust gases) with a metering pump (ISMATEC-Reglo CPF analog) and by burning it with an oxidizing honeycomb catalyst (OXICAT by Johnson Matthey) placed just upstream, from the filter in order to obtain an inlet trap temperature of about 550 °C. The time needed for the complete filter regeneration (e.g. combustion of soot hold-up) is an index of catalyst performance. The higher the catalyst activity, the lower the time required to regenerate the filter. The completeness of the regeneration process was indicated by the filter pressure drop decreasing to a value that was practically equal to or lower than that measured at the beginning of the loading phase. A twin run on a virgin, non-catalytic filter was also performed for comparison purposes.

Furthermore, the same catalyst thermal ageing procedure employed on the powders was applied to the catalytic trap, after bench testing. A standard loading-regeneration run was also carried out on this aged trap.

3. Results and discussion

Fig. 1 illustrates the diffraction spectra recorded for all the catalysts synthesized in the present study: it confirms the presence of a crystalline lanthanum cobaltite phase (JPCDS card: PDF 48-0123), which is substantially preserved after all the forced La substitutions or sub-stoichiometries. However, since the detection limit of this technique is 4 wt%, the presence of amorphous or minor crystalline phases cannot be completely excluded.

The atomic absorption analysis (AAS) confirmed that the overall amount of the various elements of interest (La, Rb, K,

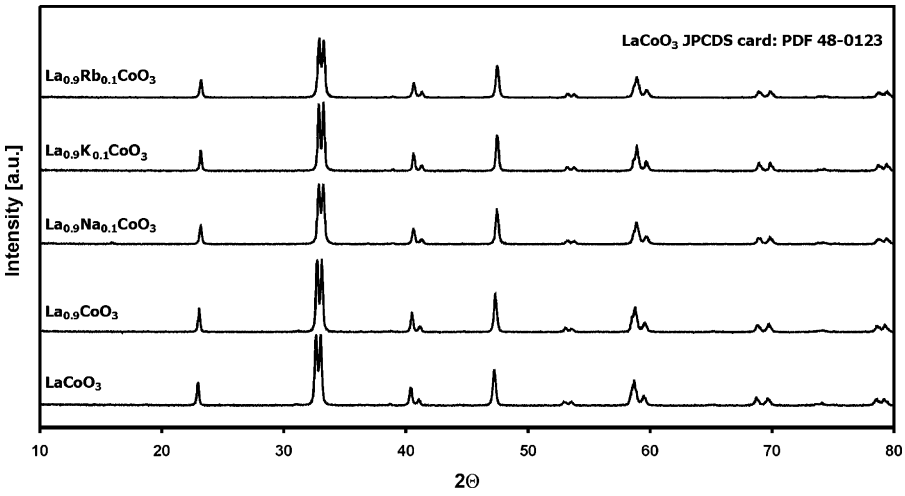

Fig. 1. XRD diffraction patterns of all the synthesized catalysts.

Na, and Co) was consistent with that used in the precursors and was compatible with the phases detected by X-ray diffraction.

Conversely, Fig. 2 shows an FESEM picture of the $La_{0.9}Rb_{0.1}CoO_3$ catalyst produced via combustion synthesis. This figure refers to the catalyst which showed the highest activity among those that were investigated, as later detailed. However, the figure is quite representative of all the prepared catalysts. Most of the perovskite crystals range between 65 and 75 nm in size, which is perfectly in line with the BET-specific surface areas measured and listed in Table 1 (about 7 m^2/g on average). It can easily be calculated, in fact, that the above range size should correspond approximately to specific surface areas in the 6–9 m^2/g range, once assumed the average density of the catalyst particles is assumed equal to 6500 kg/m^3 (an average value for tested the perovskites [37]), and a spherical shape for the particles themselves. Hence, the BET surface area should actually correspond to the geometrical surface area exposed by the perovskite crystals and no nano-scale pores should be present. It is worth mentioning that any pores below 10 nm, that dominate the specific surface area of most industrial catalysts, are of no use in the direct-contact solid–solid catalysis here pursued.

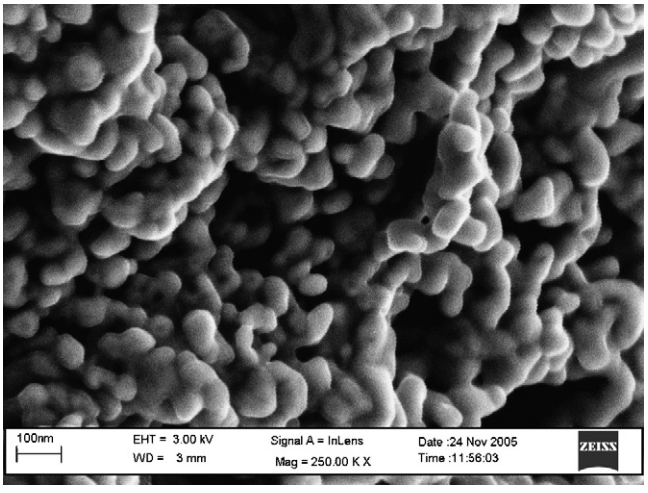

Fig. 2. FESEM micrograph of the $La_{0.9}Rb_{0.1}CoO_3$ catalyst crystals: high-magnification view (250,000×).

Finally, no indications of the possible presence of amorphous or minor crystalline phases are perceivable in Fig. 2, or in any FESEM observation made on the prepared catalysts.

The microstructure of the catalyst crystal agglomerates looks rather spongy (Fig. 3). This is a consequence of the sudden release of a large amount of gas during the combustion synthesis, due to the decomposition/combustion of the reacting precursors. Such a microstructure fosters the formation of highly corrugated interfaces of the catalyst powder agglomerates, which should result in an intensification of the contact between the catalyst and the soot. In the present context, perovskite crystals with a size of the same order of magnitude as that of the diesel particulate aggregates (on average 100 nm for last generation common-rail engines [38]) are expected to provide the highest specific number of contact points between these two counterparts.

Table 1 lists, apart from the BET-specific surface area (SSA), both the combustion onset temperature (5% soot combustion, derived form CO_2 plot integration) and the CO_2 peak temperature obtained from each tested catalyst, the activation energy values, the amount of O_2 desorbed during TPD analysis and the amount of H_2 consumed during the TPR analysis.

As expected, all the catalysts significantly lower the combustion peak temperature compared with that of the non-catalytic combustion. An activity order can be outlined as follows:

- the $La_{0.9}Rb_{0.1}CoO_3$ shows the best activity under tight contact conditions (T_p = 393 °C);
- the other substituted or sub-stoichiometric perovskite catalysts exhibit quite similar activities (T_p = 415–437 °C);
- the unsubstituted $LaCoO_3$ is the least active catalyst (T_p = 455 °C).

This activity order substantially remains preserved under loose contact conditions, although the CO_2 peak temperatures are, as expected, shifted to 55–70 °C higher values.

Table 1
Collection of results of catalyst characterization tests concerning the BET-specific surface area, activation energy, catalytic activity (loose and tight contact conditions), temperature-programmed desorption of O_2 and temperature-programmed reduction with H_2

Catalyst	BET (m^2/g)	E_a (kJ/mol)	$T_{5\%}$ tight (°C)	T_p tight (°C)	$T_{5\%}$ loose (°C)	T_p loose (°C)	Desorbed O_2 (μmol/g)	Consumed H_2 (mmol/g)	
								1st step	2nd step
$LaCoO_3$	5.9	145.2	402	455	459	518	–	1.40	2.77
$La_{0.9}CoO_3$	7.1	142.0	360	437	419	497	439.0	1.59	2.75
$La_{0.9}Na_{0.1}CoO_3$	4.9	136.4	358	427	418	491	78.1	1.53	2.78
$La_{0.9}K_{0.1}CoO_3$	7.2	131.1	345	415	407	480	63.6	1.55	2.76
$La_{0.9}Rb_{0.1}CoO_3$	8.8	110.5	330	393	388	463	65.7	1.54	2.75
Non-catalytic combustion	–	157.0	470	560	–	–	–	–	–

CO_2 selectivity for the catalyst-promoted combustion processes was always higher than 96% under close (tight) contact conditions and 91% under loose contact ones. The lower CO_2 selectivity recorded under loose contact conditions is possibly due to the influence, starting approximately above 450 °C, of direct non-catalytic oxidation pathways. The non-catalytic combustion of Printex U, which occurred at rather high temperatures, was in fact found to slightly exceed only 60% of the CO_2 selectivity.

A prerequisite for practical applicability of a catalyst is not only its activity but also its stability. Table 2 shows that no serious deactivation was found after the very severe thermal ageing test. An increase of a few degrees Celsius was noticed after the ageing treatment, although the specific surface area of the catalyst is reduced. Even after repeated combustion cycles, the activity remains almost unaffected.

The values of activation energy for carbon combustion, calculated for most of the various prepared perovskites via the Starink method (see Table 1), are not very different from one another, which seems to entail that the different perovskites are capable of delivering oxygen species of a similar nature to the reacting carbon particulate. The same type of reactive oxygen species should in fact lower the activation energy of non-catalytic soot combustion to a similar extent for all perovskites. However, a monotone relationship between T_p and E_a values can be found for most catalysts, which would seem to show that the progressively higher catalytic activity of the catalysts listed in Table 1 is somehow related to a higher reactivity of the delivered oxygen species. This should be a distinctive feature as the most active $La_{0.9}Rb_{0.1}CoO_3$ catalyst that shows clearly lower activation energy compared to those of the other catalysts. This would suggest that the oxygen species delivered by Rb-substituted lanthanum cobaltite are intrinsically much more active than those of the other catalytic counterparts.

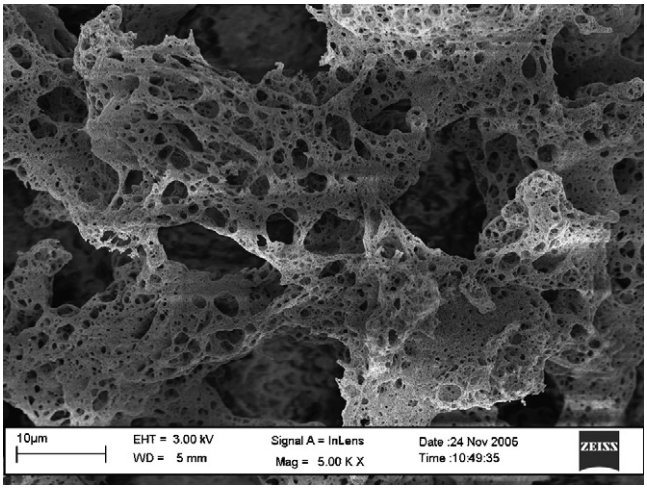

Fig. 3. FESEM micrograph of the $La_{0.9}Rb_{0.1}CoO_3$ catalyst crystals: overall view (5000×).

The transient thermal analysis studies were quite helpful to elucidate the soot combustion activity order of the prepared cobaltites. Fig. 4 shows the results of the oxygen TPD runs.

As thoroughly discussed in a review by Seyama [39] and in a number of papers (e.g., [40,41]), perovskites can desorb two different types of oxygen species at high temperatures: a low temperature species, named α, desorbed in the 300–600 °C range, and a high temperature one, named β, desorbed above 600 °C. The α desorption peak is not always perceivable in TPD plots and depends to a great extent on the concentration of surface oxygen vacancies. Its onset and intensity primarily depend on the degree of substitution of the A ion with ions of lower valence, but also on the nature of the B metal of the ABO_3 structure [42]. Conversely, the β peak is closely related to the nature of the B ion, and its occurrence is closely linked to the redox transitions of the valence state of this ion, which is cobalt in the present case.

The TPD curves in Fig. 4 suggest that no weakly chemisorbed α-type oxygen should be present on the surface of the studied cobaltites or influence the catalytic performance. If attention is focused on the temperature range below 500 °C, well inside the α oxygen region where the most active tested perovskites displayed their best soot combustion activities (see the T_p in Table 1), it can be noticed that the prepared perovskites did not display any significant oxygen desorption in this temperature range. This is a remarkable difference from the results of recent investigations by the authors on chromite-type catalysts, which were found to be almost as active as the here presented cobaltites, but were found to owe their activity to the presence of significant amounts of α-oxygen over their surface [10,33].

β-type, bulk oxygen should in fact govern the TPD behaviour of the catalysts here investigated. The highest releases of this intra-facial oxygen were indeed noticed for the $La_{0.9}CoO_3$, the catalyst characterized by the highest charge perturbation caused by the loss of one tenth of trivalent La, which was likely compensated by a corresponding shift of Co^{3+}

Table 2
Collection of results of $La_{0.9}Rb_{0.1}CoO_3$ catalyst characterization tests concerning the BET-specific surface area, catalytic activity (loose and tight contact conditions) after ageing at 850 °C and 30 vol.% of water for 16 h and after any of the nine repeated combustion cycles

Catalyst	Ageing procedure	BET (m^2/g)	$T_{5\%}$ tight (°C)	T_p tight (°C)	$T_{5\%}$ loose (°C)	T_p loose (°C)
$La_{0.9}Rb_{0.1}CoO_3$	Fresh	8.8	330	393	388	463
$La_{0.9}Rb_{0.1}CoO_3$	850 °C–30 vol.% H_2O–16 h	4.2	340	401	395	467
$La_{0.9}Rb_{0.1}CoO_3$	1st combustion cycle	8.7	337	398	394	468
$La_{0.9}Rb_{0.1}CoO_3$	2nd combustion cycle	8.7	334	393	391	463
$La_{0.9}Rb_{0.1}CoO_3$	3rd combustion cycle	8.6	335	395	393	464
$La_{0.9}Rb_{0.1}CoO_3$	4th combustion cycle	8.6	333	393	390	462
$La_{0.9}Rb_{0.1}CoO_3$	5th combustion cycle	8.4	331	389	390	461
$La_{0.9}Rb_{0.1}CoO_3$	6th combustion cycle	8.3	339	398	399	467
$La_{0.9}Rb_{0.1}CoO_3$	7th combustion cycle	7.9	325	383	384	455
$La_{0.9}Rb_{0.1}CoO_3$	8th combustion cycle	7.7	349	413	407	480
$La_{0.9}Rb_{0.1}CoO_3$	9th combustion cycle	7.6	344	403	401	474
Non-catalytic combustion	–	–	470	560	–	–

ions to Co^{4+}. This enables the possibility of releasing some bulk oxygen with a corresponding change in the valence of these Co^{4+} ions back to Co^{3+} ones. Obviously, the overall amount of released β-type oxygen species does not govern the catalytic activity, but, as previously mentioned when discussing the E_a values in Table 1, the oxygen species released in the TPD runs must have a different reactivity.

Moreover, no oxygen seems to be delivered by the basic $LaCoO_3$ perovskite, even at temperatures approaching 1000 °C. This is a sign of a rather high stability and low catalytic activity of this reference material. Conversely, the larger oxygen release associated to the $La_{0.9}CoO_3$ (see Table 1 for the amount of oxygen desorbed) could be correlated to the very high lattice distortion due to the absence of alkali metal and to the higher amount of high-valence Co needed to achieve electro-neutrality compared with the other perovskites that underwent La substitution with Na, K or Rb.

The Core level XPS spectra (Fig. 5) were measured for the most active sample, $La_{0.9}Rb_{0.1}CoO_3$, in order to evaluate the valence state of the mentioned oxygen ions, as well as those of the transition metal Co. As mentioned earlier, the sample was analysed after calcination in pure oxygen at 600 °C for 1 h (label: "600 °C O_2") and just after the second heat treatment at 400 °C in an ultra high vacuum (label: "400 °C UHV").

These two treatments were performed in order to attempt to simulate, in the XPS apparatus, the catalyst behaviour before and after the oxidation activity towards diesel soot. By comparing the XPS data regarding the two treatments and the two different regions it can be noticed that no modifications are observable in the valence state of either Co or O after both oxidation and reduction treatments. This is a further sign that, once again, the easily removable suprafacial oxygen is not involved in the catalytic carbon combustion over the cobaltites, unlike chromites [33,43].

This behaviour changes significantly when a strong reducing reactant is employed, which unfortunately could not be checked in the XPS chamber due to specific prescriptions made by the manufacturer. The TPR profiles of the cobalt-containing perovskites are reported in Fig. 6. All the perovskites showed similar reduction profiles consisting of two sets of peaks at

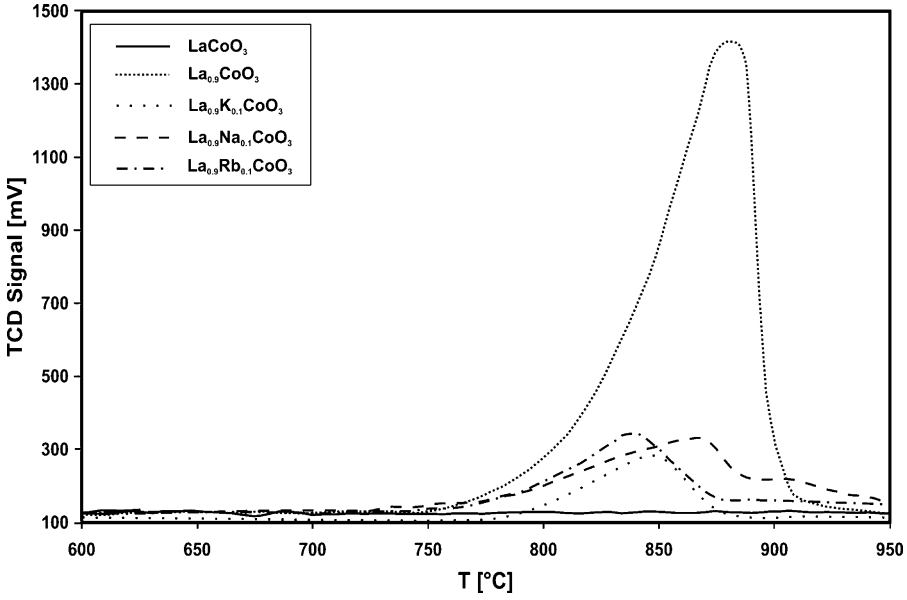

Fig. 4. Results of the oxygen TPD tests on all the investigated perovskite catalysts.

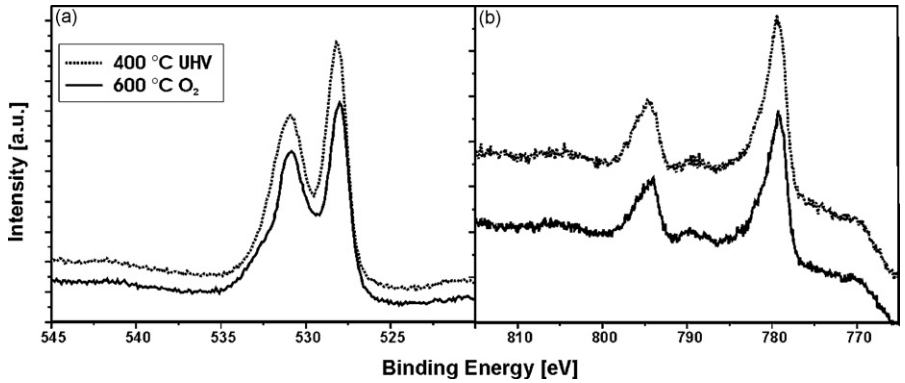

Fig. 5. X-ray photoelectron spectra in the O 1s region (a) and Co 2p region (b) of $La_{0.9}Rb_{0.1}CoO_3$: solid line = treated at 600 °C under O_2; dotted line = treated at 400 °C under ultra-high vacuum (UHV).

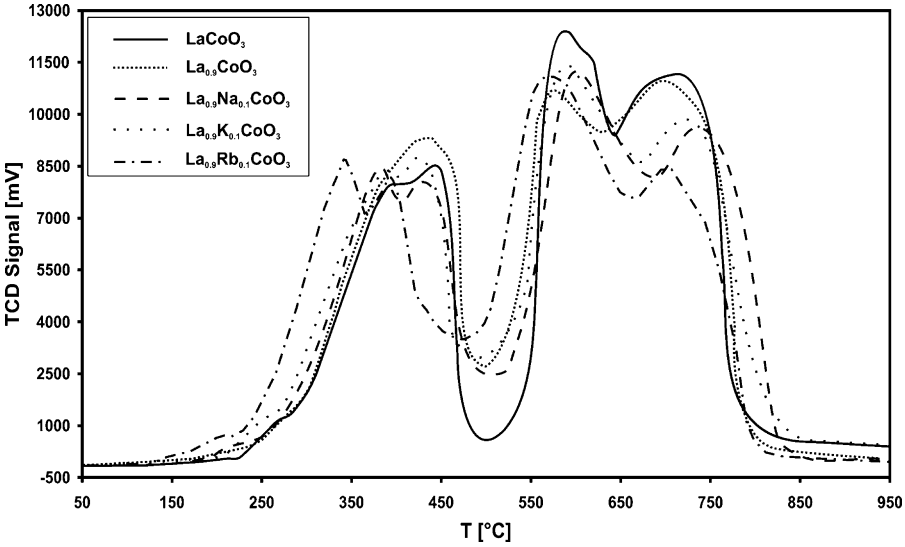

Fig. 6. Results of the TPR tests on all the investigated perovskite catalysts.

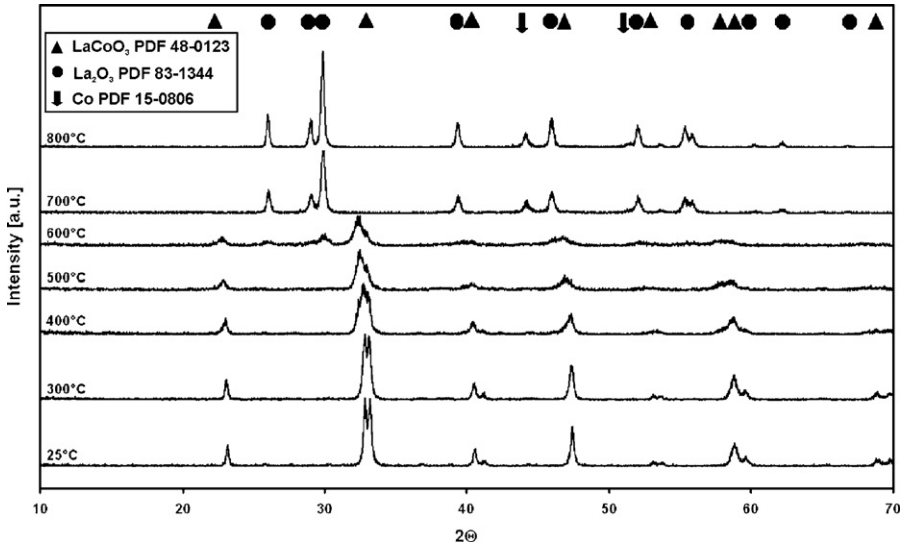

Fig. 7. XRD diffraction patterns of the $La_{0.9}Rb_{0.1}CoO_3$ catalyst at temperatures ranging from 25 to 900 °C in an reducing mixture flow of 5% H_2 in Ar.

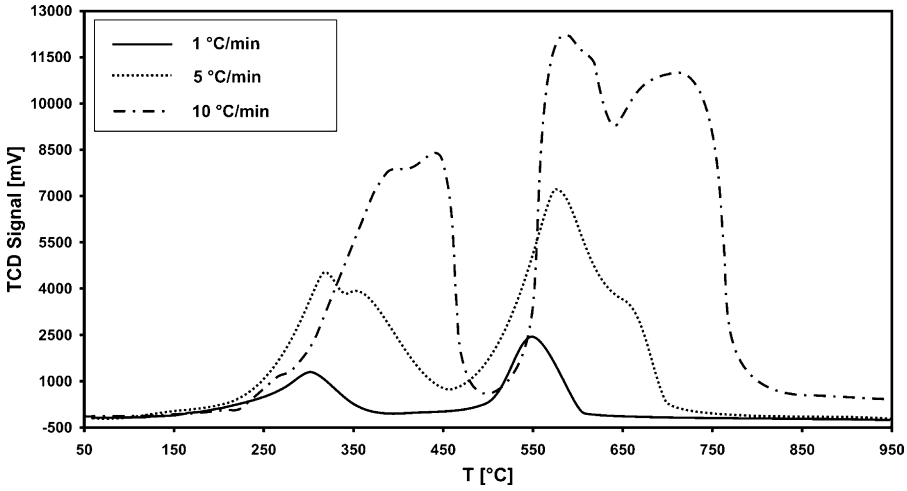

Fig. 8. Results of the TPR tests on the $La_{0.9}Rb_{0.1}CoO_3$ catalyst at 1, 5 and 10 °C/min heating rates.

approximately 400 and 650 °C. In the case of $LaCoO_3$, the hydrogen consumption for the first reduction step was approximately half of the hydrogen consumption obtained for the second reduction step (see data listed Table 1). This value was always higher for the other prepared cobaltites. The XRD data (Fig. 7) of the catalysts, after the first reduction step, showed that the perovskite structure was retained. Conversely, after the second reduction step, the XRD data showed that the perovskite structure disappeared and lanthanum hydroxide and metallic cobalt were formed. This is in line with literature data [43,44] that have demonstrated that the first step for stoichiometric cobaltite is a one-electron reduction process ($Co^{3+} + e^- \rightarrow Co^{2+}$) whereas the second step is a two-electron reduction process ($Co^{2+} + 2e^- \rightarrow Co^0$). It goes without saying that, for the other prepared cobaltites, the first reduction step Co^{4+} involves also reduction to Co^{2+}, as confirmed by the higher amount of hydrogen reacting during the first reduction step compared with the stoichiometric cobaltite. The presence of Co^{4+} was already observed and reported in [45,46]. If the activity order of the synthesized catalysts is compared with the TPR curves, regarding the first reduction step, it can be underlined that the first reduction in the B site can be indicated as the key player in the soot oxidation state. The most active catalyst for soot combustion is the one which undergoes this first reduction step at the lowest temperature, which is a sign of higher intrinsic oxygen reactivity. Moreover, the easiness of cobalt to be reduced from $Co^{3+,4+}$ to Co^{2+} by hydrogen seems to be directly correlated to the likely increasing distortions induced by the substitutions with larger alkali metals. The Shannon effective ionic radius of lanthanum is in fact 1.36 Å, whereas those of sodium, potassium and rubidium are 1.39, 1.64 and 1.72 Å, respectively [47]. Hence, the presence of the rather large Rb ion in the perovskite lattice may foster the release of active oxygen species associated to $Co^{3+,4+}$–Co^{2+} transitions towards soot.

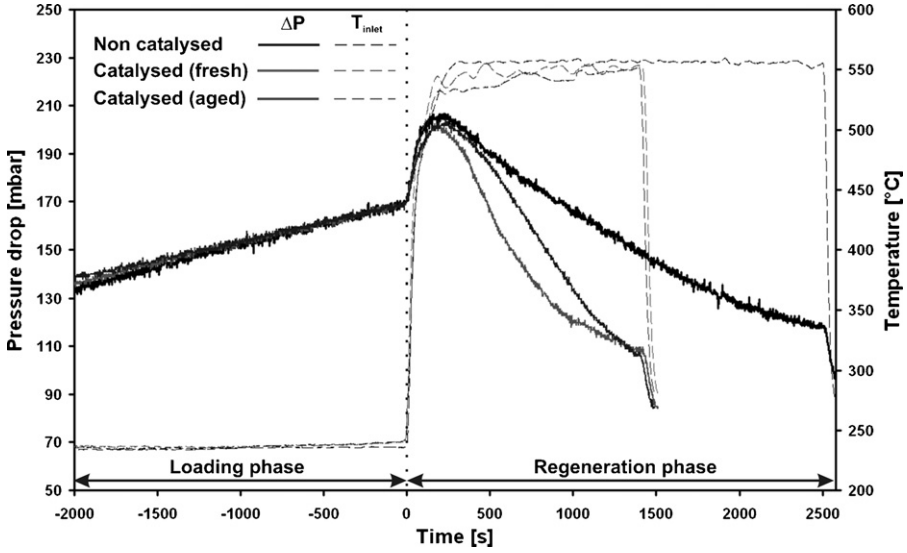

Fig. 9. Results of loading and regeneration runs for the catalysed ($La_{0.9}Rb_{0.1}CoO_3$) SiC wall-flow trap before and after the ageing treatment at 850 °C and 30 vol.% of water for 16 h and for the non-catalytic one. GHSV = 65,000 h^{-1}.

Finally, it should be underlined that the TPR profiles of both the first and second reduction steps display a double peak for all the prepared catalysts. However, the TPR run performed at lower heating rates (5 and 1 °C/min) highlighted the progressive disappearance of the two peaks (Fig. 8). In line with [45], this could indicate that the two peaks of each reduction step are probably not related to two different oxygen sites and that the reduction process is activated and probably controlled by the mass transport of H_2 and/or H_2O across the lattice.

As for the analysis of the performance of the developed trap systems, Fig. 9 compares the results of the loading (only the last part of this phase is reported to give prominence to the regeneration data) and regeneration runs performed with the fresh and aged-catalysed $La_{0.9}Rb_{0.1}CoO_3$ and the non-catalytic SiC wall-flow monolith. A striking difference can be noticed between the catalysed and the virgin traps.

By comparing the pressure drop of the catalytic and the bare trap at the same temperature it is possible to estimate a negligible effect of the catalyst layer on pore restriction. After trap loading up to a pressure drop of about 170 mbar, about 0.025 kg of fuel per kilogram of exhaust gas was post injected in both cases. This entailed a rapid increase of up to 550 °C in the inlet trap temperatures, as a common operating condition. The regeneration of the fresh $La_{0.9}Rb_{0.1}CoO_3$-catalysed trap was much faster than that of the non-catalytic ceramic filter; the soot combustion period resulted to be nearly halved (see the regeneration time evaluated from the starting point of the fuel post-injection). In this way, a significant amount of fuel could be saved at any filter regeneration, and operating costs could therefore be reduced.

As far as the effect of the ageing treatment on the trap is concerned, it did not induce any significant deactivation: just a very small increase on the time regeneration could be noticed for an equal amount of post-injected fuel (0.025 kg of fuel per kilogram of exhaust gases), although the regeneration of the fresh catalytic trap appears to be faster during the early regeneration phase.

4. Conclusions

Several cobaltite catalysts ($LaCoO_3$, $La_{0.9}CoO_3$, $La_{0.9}K_{0.1}CoO_3$, $La_{0.9}Na_{0.1}CoO_3$ and $La_{0.9}Rb_{0.1}CoO_3$) have been prepared by combustion synthesis, characterized, and tested as catalysts for diesel soot combustion. The Rb-substituted cobaltite catalyst ($La_{0.9}Rb_{0.1}CoO_3$) has exhibited the highest activity, even after a severe ageing treatment, because it is much easier to be reduced from $La_{0.9}Rb_{0.1}CoO_3$ to $La_{0.9}Rb_{0.1}CoO_{2.5}$, which have been pointed out as the key players in the soot oxidation state. A likely cause of this behaviour was pointed out in the distortions entailed by the intrusion of the rather large Rb ion at the La site in the $LaCoO_3$ perovskite lattice.

The wall-flow ceramic filter catalysed with the $La_{0.9}Rb_{0.1}CoO_3$ perovskite obtained by *in situ* SCS looks very promising, as it required half the time for trap regeneration and the related fuel penalty compared to that of a non-catalytic trap.

Acknowledgement

CORNAGLIA S.p.A. is gratefully acknowledged for hosting the engine bench tests in its facilities.

References

[1] A. Namdeo, M.C. Bell, Environ. Int. 31 (2005) 565–573.
[2] A. Schaefer-Sindlinger, I. Lappas, C.D. Vogt, T. Ito, H. Kurachi, M. Makino, A. Takahashi, Top. Catal. 42/43 (2007) 307–317.
[3] Summary of worldwide diesel emission standards, http://www.dieselnet.com.
[4] M.V. Twigg, Appl. Catal. B: Environ. 70 (2007) 2–15.
[5] H. Luders, P. Stommel, R. Backes, SAE Tech. Paper 970470 (1997).
[6] S. Liu, A. Obuchi, J. Oi-Uchisawa, T. Nanba, S. Kushiyama, Appl. Catal. B: Environ. 30 (2001) 259–265.
[7] K. Kimura, T.L. Alleman, S. Chatterjee, K. Hallstrom, SAE Tech. Paper 2004-01-0079 (2004).
[8] N.K. Labhsetwar, A. Watanabe, R.B. Biniwale, R. Kumar, T. Mitsuhashi, Appl. Catal. B: Environ. 33 (2001) 165–173.
[9] D. Fino, E. Cauda, D. Mescia, N. Russo, G. Saracco, V. Specchia, Catal. Today 119 (2007) 257–261.
[10] N.K. Labhsetwar, A. Watanabe, T. Mitsuhashi, Appl. Catal. B: Environ. 40 (2003) 21–30.
[11] Y. Teraoka, S. Kagawa, K. Nakano, W.F. Shangguan, Catal. Today 27 (1996) 107–113.
[12] N. Russo, D. Fino, G. Saracco, V. Specchia, J. Catal. 229 (2005) 459–469.
[13] D. Fino, N. Russo, G. Saracco, V. Specchia, J. Catal. 217 (2003) 367–375.
[14] D. Fino, N. Russo, E. Cauda, G. Saracco, V. Specchia, Catal. Today 114 (2006) 31–39.
[15] W.F. Shangguan, Y. Teraoka, S. Kagawa, Appl. Catal. B: Environ. 8 (1996) 217–227.
[16] D. Fino, N. Russo, G. Saracco, V. Specchia, J. Catal. 242 (2006) 38–47.
[17] D.W. McKee, Carbon 8 (1970) 623–635.
[18] D.W. McKee, Carbon 8 (1970) 131–139.
[19] A.F. Ahlstrom, C.U.I. Odenbrand, Appl. Catal. 60 (1990) 157–182.
[20] M.L. Pisarello, V. Milt, M.A. Peralta, C.A. Querini, E.E. Miro, Catal. Today 75 (2002) 465–470.
[21] W.F. Shangguan, Y. Teraoka, S. Kagawa, Appl. Catal. B 16 (1998) 149–154.
[22] Y. Watabe, K. Yrako, T. Miyaijma, T. Yoshimoto, Y. Murakami, SAE paper no. 830082 (1983).
[23] D. Fino, N. Russo, C. Badini, G. Saracco, V. Specchia, AIChE J. 49 (2003) 2173–2180.
[24] P. Ciambelli, V. Palma, P. Russo, S. Vaccaro, J. Mol. Catal. A: Chem. 204/205 (2003) 673–681.
[25] R.E. Mariangeli, E.H. Homier, F.S. Molinaro, Catalysis and Automotive Pollution Control, Elsevier, Amsterdam, 1987.
[26] E.S. Lox, J. Van den Tillaart, L. Leyrer, S. Eckhoff, Appl. Catal. B: Environ. 10 (1996) 53–68.
[27] A. Civera, M. Pavese, G. Saracco, V. Specchia, Catal. Today 83 (2003) 199–211.
[28] K.C. Patil, S.T. Aruna, S. Ekamaram, Curr. Opin. Solid State Mater. Sci. 2 (1997) 158–165.
[29] K.C. Patil, S.T. Aruna, T. Minami, Curr. Opin. Solid State Mater. Sci. 6 (2002) 507–512.
[30] D. Fino, V. Specchia, Chem. Eng. Sci. 59 (2004) 4825–4831.
[31] B.R. Stanmore, J.F. Brilhac, P. Gilot, Carbon 39 (2001) 2247–2268.
[32] K.-H. Choi, Y. Korai, I. Mochida, Comb. Flame 137 (2004) 255–260.
[33] Y.N.H. Nhon, H.M. Magan, C. Petit, Appl. Catal. B: Environ. 49 (2004) 127–133.
[34] P. Palmisano, N. Russo, P. Fino, D. Fino, C. Badini, Catal. Appl. B: Environ. 69 (2006) 85–92.
[35] D. Mescia, E. Cauda, N. Russo, D. Fino, G. Saracco, V. Specchia, Catal. Today 117 (2006) 369–375.
[36] M.J. Starink, Thermochim. Acta 288 (1996) 97–104.

[37] R.H. Perry, D.W. Green, J.O. Maloney, Perry's Chemical Engineers' Handbook, VI ed., McGraw-Hill Book Co., New York, 1984.
[38] M. Kostoglou, P. Housiada, A.G. Konstandopoulos, Chem. Eng. Sci. 58 (2003) 3273–3283.
[39] T. Seyama, Catal. Rev.-Sci. Eng. 34 (1992) 281–300.
[40] N. Yamazoe, Y. Teraoka, Catal. Today 8 (1990) 175–199.
[41] G. Saracco, F. Geobaldo, G. Baldi, Appl. Catal. B: Environ. 20 (1999) 277–288.
[42] L. Forni, I. Rossetti, Appl. Catal. B: Environ. 38 (2002) 29–37.
[43] L. Lisi, G. Bagnasco, P. Ciambelli, S. De Rossi, P. Porta, G. Russo, M. Turco, J. Solid State Chem. 146 (1999) 176–183.
[44] R. Lago, G. Bini, M.A. Peña, J.L.G. Fierro, J. Catal. 167 (1997) 198–209.
[45] P. Wang, L. Yao, M. Wang, W. Wu, J. Alloys Compd. 311 (2000) 53–56.
[46] J.C. Dupin, D. Gonbeau, H. Benqlilou-Moudden, Ph. Vinatier, A. Levasseur, Thin Solid Film 384 (2001) 23, 32.
[47] www.webelements.com.